Algorithm-driven DNA nanostructure design for advanced functionality

Nicolas Levy[1,†] Julie Finkel[2,†] Allan Mills[2] Gerrit David Wilkens[2]
Anjelica Kucinic[2] Aurélie Ancelin[2] Pierre Marcus[1] Octave Hazard[1]
Joris Picot[1] Daria Pchelina[1] Gaëtan Bellot[2,*] Nicolas Schabanel[1,3,*]

September 15, 2025

[1] LIP, École Normale Supérieure de Lyon, France, `http://perso.ens-lyon.fr/perso/first.lastname`
[2] CBS, Université de Montpellier, France.
[3] CNRS, IXXI, École Normale Supérieure de Lyon, 46 allée d'Italie, 69364 Lyon Cedex 07, France.
[†] These authors contributed equally to this work
[*] Corresponding authors: `nicolas.schabanel@ens-lyon.fr` and `gaetan.bellot@cbs.cnrs.fr`

Abstract. Form and function are intimately linked—a guiding principle across both biology and engineering. While evolution and human ingenuity have shaped this landscape through function-driven form selection, AI-driven generative design expands it beyond natural and intuitive geometries, enabling the exploration of structure-driven functionalities that were previously inaccessible. At the nanoscale, however, realizing such non-intuitive architectures remains a key challenge, limiting the development of multifunctional nanostructures across biology, chemistry, and materials science. To address these constraints, we introduce an algorithmic design paradigm that enables DNA helices to follow non-planar 3D trajectories, thereby supporting the structural and functional outcomes required for advanced capabilities. We implemented this paradigm in ENSnano, a software platform that integrates mathematical models to automate structural design in 3D space without the need of human intervention. This framework allows us to rapidly generate DNA nanostructures with key functional features such as curvature, encapsulation, and hierarchical organization—reminiscent of naturally occurring biological architectures. As a key application, we demonstrate an automated pathway from biological to engineered structures by designing and experimentally assembling Vault-like cages directly derived from the emPDB model of the Vault protein, marking a step forward in biomimetic DNA nanostructure design.

One-sentence summary. Algorithms enable accurate design of DNA origami nanostructures with complex 3D curvature and torsion.

Introduction

The interplay between form and function is a unifying principle across natural and engineered systems. In engineered gears, specific geometries optimize force transmission, while in architectural arches, curvature and torsion enhance structural rigidity and stability[1,2]. Many of engineered designs draw inspiration from biology, where evolution has refined structural forms to achieve specific functional outcomes[3]. Advances in artificial intelligence and generative design now enable the creation of structural designs that depart from both evolutionary precedent and human intuition, thereby expanding the accessible form–function landscape[4].

Translating these functional forms to the nanoscale presents a significant challenge, requiring molecular-level precision to ensure function, an essential step toward the development of smart materials, synthetic biological systems, and precision therapeutic devices. Structural DNA nanotechnology addresses this challenge by redefining nucleic acids as programmable building blocks for encoding functional shapes at the nanoscale[5].

Among self-assembly strategies, DNA origami[6] has become the benchmark for constructing accurate nanoscale architectures. It enables precise control over geometry, site-specific chemical functionalization, and dynamic mechanical properties[7,8,9,10], while producing bil-

lions of copies in a single-pot reaction. In this approach, a long single-stranded DNA scaffold is folded into a target shape by hundreds of short oligonucleotides through sequence-specific base pairing. This programmable assembly method has facilitated the creation of diverse nanostructures, advancing both biological research and materials science by encoding functional form at the molecular scale[11,12,13].

However, current design strategies remain largely restricted to geometries composed of straight segments[14,15,16] and planar arcs[17,18]. This constraint arises from the conventional DNA origami approach, which models helices as near-rigid cylinders connected by crossovers at fixed spacing. The reliance on fixed crossover spacing cannot accommodate the non-integer helical twist of DNA[19,20], which is approximately 10.44 base pairs per turn[21,22,23]. Furthermore, classical geometric approaches[24] often introduce unintended helical twist when mapping DNA onto non-planar curves. As a result, current frameworks support only planar arrangements of helices and break down when non-planar trajectories involving both curvature and twist are required. Yet such trajectories are essential for expanding the accessible design space, as many functional structures in biology and materials science exhibit non-planar three-dimensional curves and twisted geometries[1,2].

Here, we introduce an algorithm-driven design framework that enables the construction of DNA origami structures with helices arranged along non-planar trajectories in three-dimensional space. This approach allows precise crossover placement and promotes uniform strain distribution across helices while minimizing torsional stress. Our approach integrates three core elements (Fig. 1): a nucleotide positioning algorithm for non-planar 3D curves, automated computation of helix trajectories to cover target shapes, and structural optimization routines to relieve strain in the design. This algorithmic workflow—automating the most time-consuming aspects of curved DNA nanostructure design[18]—is fully integrated into our open-source software, ENSnano[25,26]. Using this framework, we designed and assembled previously inaccessible nanostructures, including curved helical bundles in three-dimensional space, twist-rich hollow architectures, and nested spherical shells connected by narrow tunnels. These structures demonstrate key functional attributes—such as mechanical robustness, molecular encapsulation, compartmentalized reactivity, and channel-like features that regulate inter-compartmental transport and flow—commonly observed in biological systems.

As a direct application, we designed an artificial nanostructure that mimics the geometry and dimerization behavior of the Vault protein by generating a DNA origami nanocage with geometry automatically derived from the protein's atomic model in the Protein Data Bank (PDB). This biomimetic construct demonstrates how computational control over nanoscale curvature and twist enables the rational design of functional, bioinspired architectures that transcend the geometric constraints of conventional DNA origami.

Results

Algorithmic nucleotide positioning along arbitrary 3D curves. Mapping a DNA helix onto a non-planar 3D curve requires defining a moving frame along the curve. The classical Frenet frame approach[24] fails in this context, as it rotates erratically under the influence of torsion in non-planar curves, introducing unwanted twist into the mapped helix. To address this, we developed a custom algorithm that computes a lazily rotating moving frame along the curve (algorithm SA1). We then use the computed frame to map the DNA helix onto the curve using the best-known structural parameters for DNA[22] (table ST1 and fig. S1). Figure S2 illustrates the algorithm in action, while Figure S3 compares the classical Frenet frame to our approach. The comparison demonstrates that our algorithm avoids unnecessary frame rotation, producing a minimally twisted DNA helix with a more regular twist, closer to its canonical value in the straight conformation.

We validated our DNA model by simulating a nucleosome, a key example of DNA curvature in biology. In the nucleosome, the DNA helix undergoes significant bending, wrapping approximately 1.65 turns around the histone octamer to form a left-handed superhelix[27]. Figure S4 compares crystallographic data (`2CV5.PDB`) with the output of our algorithm for a DNA helix wound around a nucleosome. Our model accurately reproduces nucleotide positions with an RMSD of 0.54 ± 0.23 nm, and phosphate with an RMSD of 0.44 ± 0.22 nm (figs. S5 and S6).

DNA helix bundle non-planar curvature programming. DNA helix bundles are a fundamental component of the DNA origami design toolbox. Early design strategies[14,18] laid the groundwork for a wide range of applications, including nuclear pore complex mimics[28], liposome templating[29], membrane shaping[11], spring-loaded nanodevices[30], and targeted drug delivery systems[13]. Here we present an algorithm that

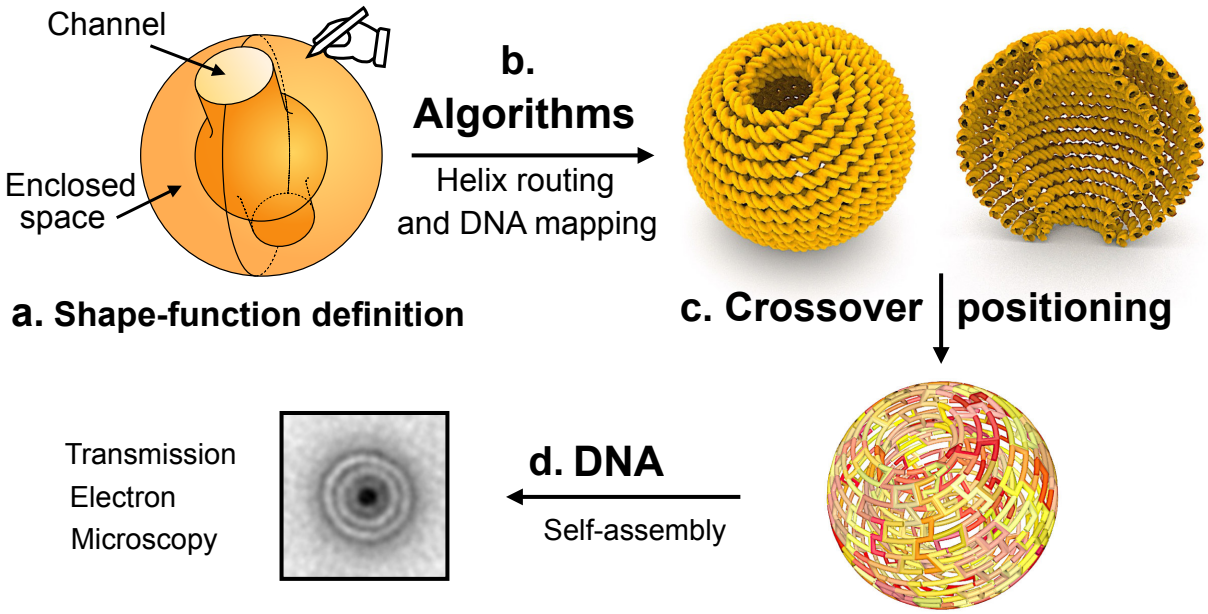

Figure 1: Algorithm-driven conceptual framework for DNA nanostructure design. (a) The target shape is defined using Bézier curves and geometric descriptors, such as the revolution surface tool. (b) The algorithm automatically computes helix trajectories that cover the target shape at an appropriate scale for the chosen scaffold strand, positioning nucleotides along their (possibly non-planar) 3D paths. A series of automated optimizations is applied to relieve structural strain. (c) The designer places scaffold and staple strand crossovers between helices. (d) Staple strand sequences are exported for assembly and imaging. Shown here is a negative-stain 2D TEM class average of the resulting self-assembled DNA nanostructure, box size is 80×80 nm.

enables the design of curved helix bundles in full 3D space, with continuously varying radii of curvature.

In our approach, a DNA helix bundle is defined by attaching a grid (square or honeycomb) to a Bézier curve $t \mapsto M(t)$. Each helix, located at coordinates (i, j), follows the path $t \mapsto P_{ij}(t)$ of the grid point at coordinates (i, j) in the moving frame $\mathbf{F}(t)$ centered on $M(t)$ (fig. S7). This construction ensures that the trajectories of the helices remain uniformly spaced along the entire length of the bundle. DNA helices are then mapped in real time onto their respective paths $P_{ij}(t)$ using the previously described DNA model. A core feature is that, since all helices in the bundle evolve along the common parameter t, we introduced an adaptive 2D view of the structure in ENSnano software. In this 2D representation, the width of each nucleotide's cell is automatically adjusted based on t, ensuring that all nucleotides at the same cross-section appear vertically aligned (fig. S8). As a result, nucleotides eligible for crossovers are naturally aligned in the 2D view, eliminating the need for manual insertions or deletions. For closed curves, the rise and helicity of each DNA helix are automatically adjusted to ensure an integer number of helical turns. In practice, these adjustments are minimal (only a few ‰) and remain well within established precision limits. This optimization helps to evenly distribute mechanical strain along each DNA helix (figs. S9 to S12). All calculations are performed in real time, enabling the designer to interactively fine-tune the curve, either to precisely position functional groups or to ensure an *exact* match with the scaffold length.

Then, we proceed to position the crossovers by first placing a single crossover between adjacent helices. Next, we apply our *auto-roll* algorithm, which rotates neighboring helices to minimize crossover lengths. Once the helices are rotationally aligned, a standard scaffold and staple pattern is applied, with crossover positions visually adjusted in both 2D and 3D views of the design to optimize their length and orientation.

To explore the effectiveness of our method we designed a four-loop DNA origami structure, referred as ⌘-origami. The ⌘-origami consists of a 6-helix bundle programmed with four precise 270-degree looped bends (figs. S13 to S18). The crossover patterns were selected to minimize structural strain by 1) spacing the scaffold crossovers approximately every 100 base pairs, and 2) reducing the occurrence of double crossovers for the staples. The scaffold layout follows a "leaf" pattern (fig. S19), where each domain or "leaf" averages around 86 base pairs in length. Staples follow the classic C-shape (fig. S20), with domains typically ranging from 15 to 20 base pairs in straight regions. To ac-

commodate curvature, staple domains on the inner side of the curve may be shortened by a full turn while those on the outer side may be extended by a full turn – adjusting lengths by approximately 8 to 12 bps depending on curvature. These modifications are guided by inspection of the 3D nucleotide mapping in the interactive 3D view. In our design, staple domains range from 7 to 30 base pairs, with staple strand lengths between 19 and 60 base pairs. Crossover lengths range from 0.65 nm and 1.7 nm according to our model. After optimizing folding conditions via agarose gel electrophoresis and negative-stain TEM (ns-TEM) particle analysis, optimal folding was achieved by mixing the scaffold with staple oligonucleotides at a 10-fold molar excess, in the presence of 20 mM $MgCl_2$, and following a 42-hour temperature annealing protocol (Fig. 2 and figs. S21 to S23). ns-TEM particle analysis yielded 2D class averages that closely match the intended four looped bends, each forming a precise 270-degree angle, confirming successful folding of the structure. To further assess the fidelity of curvature programming conferred by the global crossover pattern, we introduced several structural variants: (1) opening a section of the 6-helix bundle by splitting the staple strands joining the scaffold at its termini (fig. S24), and (2) splitting the vertical staples linking the top and bottom scaffold domains at the four crossover points—designated NW, SW, SE, and NE—to decouple the vertical connection (fig. S25). Each variant yielded folded structures consistent with the degrees of freedom introduced by the respective modifications, with shape outcomes analogous to those achievable by a flexible plumbing pipe making four 270° turns (see section S2.5 and figs. S26 to S35).

Optimization of helix torsion and trajectories in hollow shapes. Designing DNA origami in capsule-like shapes is crucial for advancing nanotechnology, offering a protective barrier between the internal volume and the external environment. These 3D DNA nanostructures are finding applications in areas such as mimicking natural capsids for antigen presentation, virus trapping, low-volume reactors, templated assembly, molecular transport, and drug delivery[31,13]. Optimal functionality in these applications often depends on the creation of curved 3D hollow shapes. Previous methods for designing such structures typically involved slicing them into a stack of parallel concentric circles[18,17]. However, this approach has two main drawbacks[18]: First, the angles between adjacent layers are limited to the multiples of $\sim 34^\circ$, corresponding to the angle between two consecutive nucleotides. Second, the perimeter of each DNA ring must correspond to an integer number of full DNA helix turns. Moreover, this technique is only applicable to simple revolution surfaces[17].

One of the most challenging steps in hollow DNA origami design is determining the trajectories of the DNA helices. A small miscalculation in helix placement or torsion can lead to significant deviations in the structure, affecting both its stability and functionality. This task involves solving a multicriteria optimization problem that determines the appropriate number of helices and the scale of the shape, ensuring that the helices are uniformly spaced (with an average interdistance of 2.65 nm[6,32]), minimally curved or twisted, and that their total length matches the target size of the scaffold. This step was highlighted as the most time-consuming in previous approaches[18]. To address this, we introduce a *spiral-based* algorithm for slicing a revolution surface (possibly twisted) into curved, equally wide stripes. This method overcomes both of the aforementioned limitations of using concentric circles in two key ways, as detailed in the supplementary text (section S3). By allowing the curvature radius to vary continuously along the trajectories, our method enables a continuous range of crossover angles between adjacent helices. Moreover, since only a few long spirals (only 2 in our designs) are needed to assemble the shape, adjusting the helix parameters by a few negligible ‰ allows for continuous rescaling (figs. S36 to S38). This results in an automatic computation of the ideal scale for the target shape, optimizing the use of every single nucleotide in the scaffold. Finally, the use of spirals allows for seamless design of tubular portions with inner radii as small as 4.3 nm within a larger shape.

Our method is integrated in ENSnano software as an automatic pipeline. We proceed by specifying the surface and spirality parameters. The surface is given by its section curve, the number of twists, and its revolution radius. The spiral parameters include the number of spirals covering the surface, the *winding* parameter which dictates the rate at which the spirals coil around the surface and controls their inclination and torsion (figs. S39 and S40), and the target scaffold strand length. Our algorithm calculates the spiral trajectories for the helices using a dedicated spring system which keeps them as straight and evenly spaced as possible, minimizing their torsion along the way, as demonstrated in fig. S41. The algorithm scales the shape (section and revolution radius) until the distance between adjacent helices and the total helix length match the desired crossover distance and target scaffold length. The entire process is completed in a few

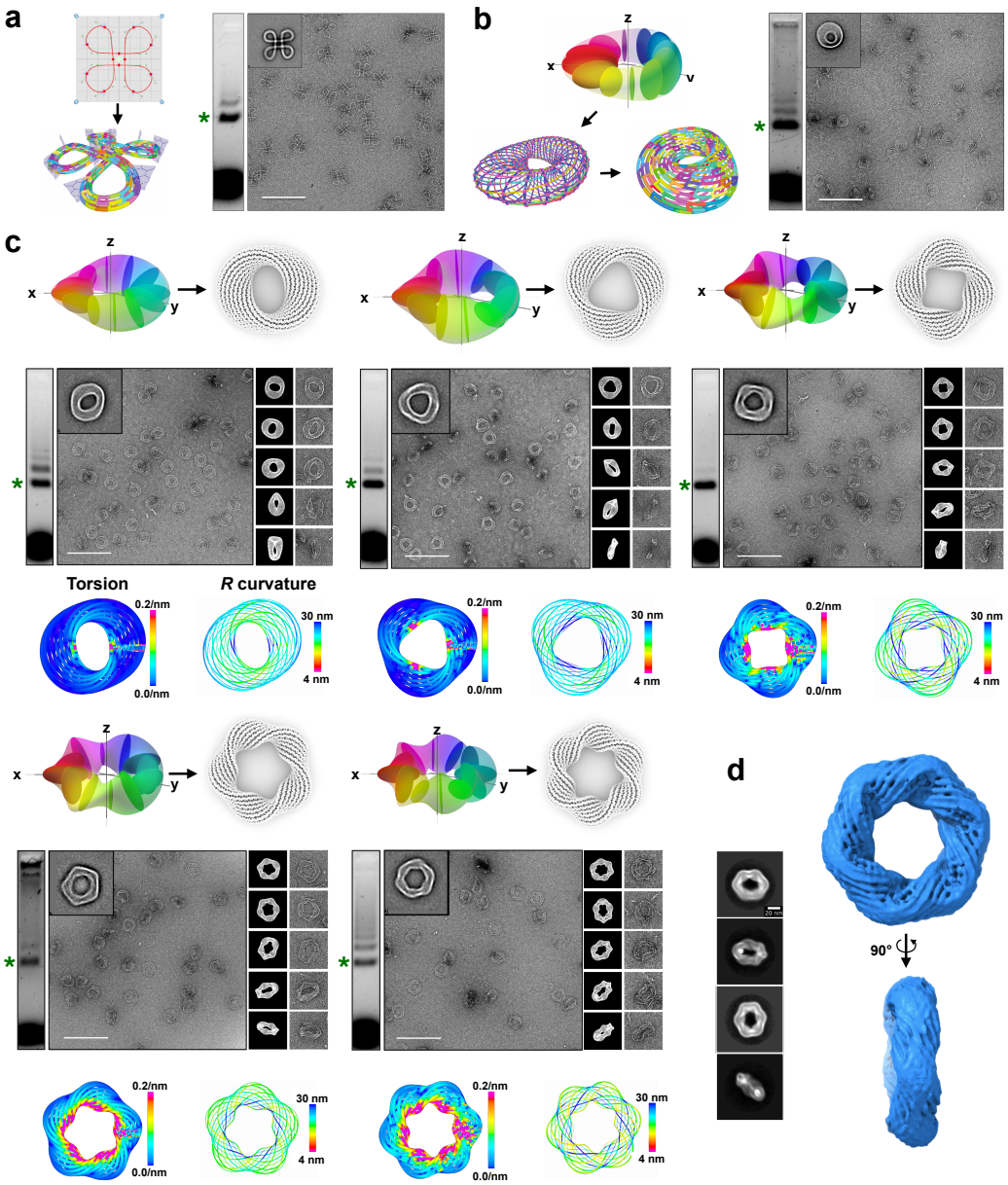

Figure 2: Spiral design algorithm for intricate hollow shapes. (a) Design workflow for a curved DNA origami composed of a 6-helix bundle with four programmed loops. In ENSnano, the bundle's Bézier path is first drawn and adjusted by the user, followed by algorithmic nucleotide mapping and crossover placement to produce the final assembly. (b) Design workflow for a half-twisted torus, defined in ENSnano as the surface generated by rotating a 2×1 ellipse by half a turn around the revolution axis. A spring-based system then optimizes helix trajectories and iteratively scales the surface until the total length matches the target scaffold length (here, 7560 bases), enabling automated nucleotide mapping and crossover placement. (c) Progressive increase in overall twisting complexity from T2 to T6, with schematic representations followed by algorithmic DNA helix routing, nucleotide mapping, and crossover placement. Below each TEM micrograph: Left: local torsion; Right: curvature radius along helices (color scales: $0\,\mathrm{nm}^{-1}$ [pink] to $0.2\,\mathrm{nm}^{-1}$ [dark blue] for torsion; and $4\,\mathrm{nm}$ [pink] to $30\,\mathrm{nm}$ [dark blue] for curvature). (d) Class averages from single particles observed with cryo-TEM and 3D reconstruction of T6 from $72\,684$ particles. For each structure, a 1% agarose gel (post-folding) and TEM micrographs are shown, alongside reference-free class averages from single particles (particle sets available in figs. S82, S86 to S88 and S92). White bars represent 200 nm; box sizes for projections and class averages are $112 \times 112\,\mathrm{nm}$ for the four-loop DNA origami and $99 \times 99\,\mathrm{nm}$ for the Tori.

seconds.

Inspired by the prevalence of twisted features in nature[33], we investigated the robustness of our spiral routing algorithm by designing a series of six toroidal structures referred as T1,...,T6 with progressively increasing torsion. The surface of Tk is obtained by rotating a 2-by-1 ellipse around a revolution axis while applying k half-turn twists to the section, as depicted in Fig. 2. Our algorithm generated, for

each of them, a pair of spiraling helices that are evenly distributed across the surface, and whose total length precisely matches the target scaffold size (7560 nucleotides). By selecting appropriate winding parameters, we minimized the torsion of the resulting helices, yielding smooth and uniform trajectories throughout the structures (figs. S41 and S42). The resulting helices complete 7 (T5 and T6), 8 (T3 and T4), 9 (T2), and 10 coils (T1), while maintaining an interaxis spacing of $2.65\,nm \pm 10\%$ relative to their counterparts.

As for the ⌘-origami, we optimized the staple and scaffold crossover placements using the 3D and 2D live-editable views provided by our algorithms (figs. S43 to S78).

We studied the assembly of T1 by combining 20 nM scaffold with a 10-fold excess of staple oligonucleotides, varying magnesium concentrations (2–$30\,mM$) over a 42-hour folding ramp. Agarose gel electrophoresis (fig. S79) identified 12 mM as the optimal magnesium concentration. ns-TEM particle analysis yielded 2D classifications in close agreement with the T1 structure model (Fig. 2). We optimized the self-assembly protocol for each structure T2 through T6, as detailed in the supplementary text. Agarose gel electrophoresis, ns-TEM particle analysis, and 2D class averaging revealed uniform particle distribution and orientation, consistent with simulated 2D projections, and demonstrating proper folding relative to the predicted shapes (Fig. 2 and figs. S80 to S92). We further validated the T6 design using cryo-TEM imaging, generating a 3D electron density map through single-particle cryo-TEM analysis (Fig. 2 and figs. S84 and S85). The map revealed the characteristic six twists per ring, confirming the structural integrity of the design.

Algorithmic surface design with curvature inversion and tunnels. We further tested the robustness of our algorithms by designing an additional structure, double sphere DS, which explores novel architectural possibilities. This design features two nested spheres in a convex-concave configuration, interconnected by narrow channels. The resulting structure includes a hermetic compartment between the inner and outer spheres, as well as an internal open compartment regulated by tunnel diameters.

Our algorithms computed evenly spaced, spiraling helices that span this structure, which were defined as the revolution surfaces generated by rotating a ☾-shaped section around an axis. DS consists of two twisted DNA helices forming an outer sphere (41 nm diameter) connected by two 10 nm-wide channels to an inner sphere (29 nm diameter). The design was automatically adjusted to match the scaffold length (8,064 nucleotides) (Fig. 3 and figs. S93 to S98). The helices form 17 coils each. After optimizing folding conditions (see supplementary text and fig. S99), optimal assembly was achieved with 30 mM $MgCl_2$ over 42 hours, confirmed by agarose gel electrophoresis and ns-TEM analysis. 2D classifications revealed a homogeneous particle distribution, distinct contrast between spheres, and clear channel structures (Fig. 3 and fig. S100).

Biomimetic DNA origami design. We explored the bio-inspired applications of our algorithms, by designing a DNA origami that mimicks the shape of the vault protein, a barrel-shaped ribonucleoprotein complex found in the cytoplasm of eukaryotic cells. The vault protein can dimerize to form a closed cage[34,35,36]. Its unique architecture and potential applications in targeted drug delivery and nanomaterial scaffolding have attracted considerable interest in nanotechnology[37].

To create the design, we began by modelling the cross-sectional curve of the vault protein PDB model 4V60 as a Bézier curve and applied our spiraling algorithm to generate the corresponding revolution surface. The shape was scaled automatically by a factor of 1.4 horizontally and 1.3 vertically, to match the target scaffold size of 8064 nucleotides, resulting in a structure 53 nm in width and 42 nm in height. Two inner hems were included at the top and the bottom of the structure to conceal the blunt ends of the helices and stabilize the 8.6 nm-wide tight hole at the top. The resulting two helices make 13 coils each. Additionally, the bottom of the design was equipped with six equally spaced 18-nucleotide anchor strands to facilitate homodimerization. The resulting design, referred as vault origami (figs. S101 to S106), was then validated through direct comparison with the Vault protein model, imported in our software as an STL file generated by Chimera from the PDB file (Fig. 4).

We optimized folding of the vault monomer using agarose gel electrophoresis and ns-TEM, identifying 20 mM $MgCl_2$ as optimal (fig. S107). As detailed in the supplementary text and figs. S108 to S112, optimal dimerization was achieved by incubating gel-purified monomers at 37°C for 15 hours, yielding dimer structures consistent with the design, as confirmed by ns-TEM and 2D class averaging (Fig. 4 and fig. S112).

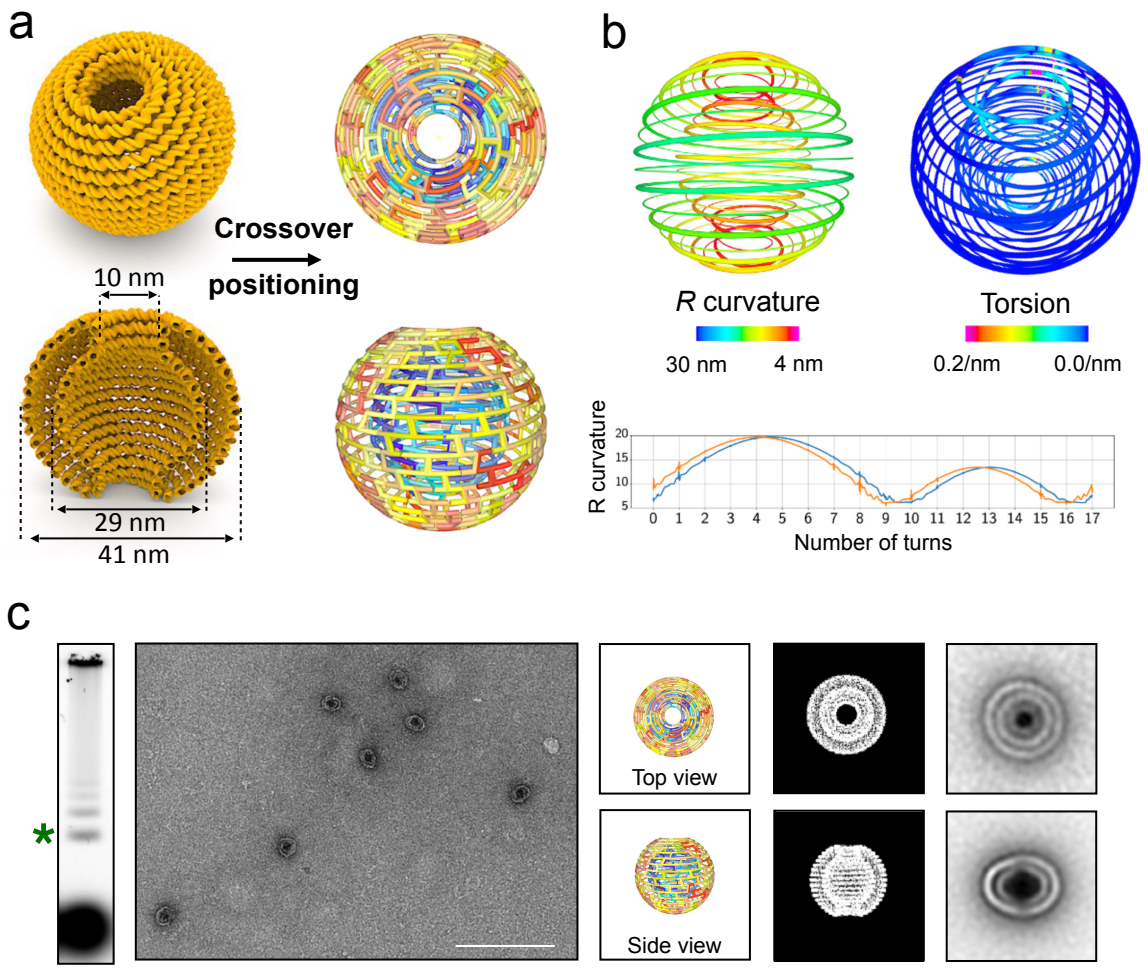

Figure 3: Spiral-based design for spherical surfaces. (a) Schematic illustration and staple design of DS. (b) Left: curvature radius along the two twisted DNA helices in DS. Right: local torsion. Color scales: 4 nm [pink] to 30 nm [dark blue] for curvature and $0\,\mathrm{nm}^{-1}$ [pink] to $0.2\,\mathrm{nm}^{-1}$ [dark blue] for torsion. Graphs show the evolution of curvature radius (in nm) as a function of the number of turns along each helix. (c) 1% agarose gel after folding and TEM micrographs of the purified band (green star), with representative projections from 3D PDB model and reference-free class averages from single particles (particle sets available in fig. S100). Scale bar represents 200 nm.

Discussion

Detailed analysis of our designs reveals that crossover spacing does not correlate with either local curvature radius or helix torsion, as shown in figs. S113 to S120 and further detailed in Supplementary Section S8. This observation highlights a critical limitation of classical rule-based design strategies[19,18], which rely on fixed patterning that cannot accommodate the geometric complexity of non-planar curved structures.

As DNA nanostructures evolve to encode increasingly sophisticated forms and functions, existing design constraints call for more advanced algorithmic strategies. Our algorithm-driven paradigm addresses this challenge by enabling non-planar curvature within DNA helix bundles and single-layer architectures, without requiring human intervention, thereby supporting greater functional intricacy. It also enhances planar designs by reducing reliance on iterative post-experimental adjustments[20], and paves the way for the scalable assembly of larger functional structures with fewer components than multi-layered composites[12]. This design framework is available through our open-source software, ENSnano[38], which integrates algorithmic control of helix geometry with intuitive 2D and 3D visualization, real-time editing, and a user-friendly interface. ENSnano is designed for continuous development, with planned extensions to support hybrid architectures—including DNA/RNA and DNA/protein systems—further bridging natural and engineered nanoscale assemblies. Finally, just as the design of a rectangle[21] in caDNAno allowed refine the pitch of straight helical DNA from 10–11 bp/turn to the now-standard 10.44 bp/turn, our framework provides

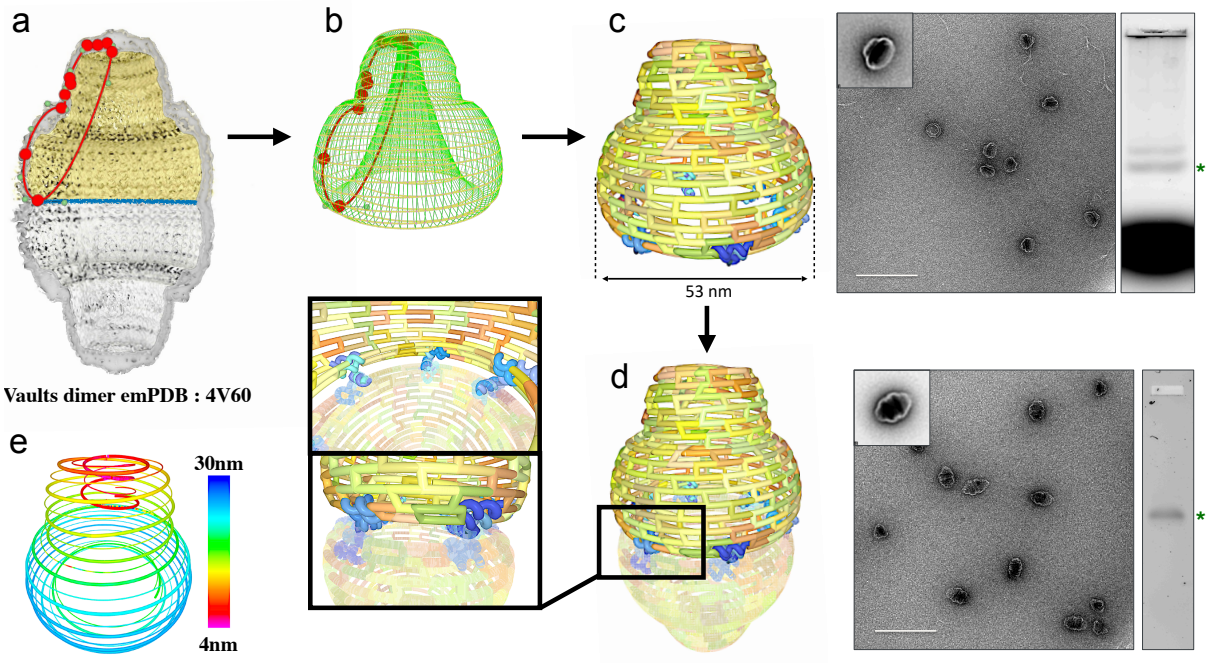

Figure 4: Bio-inspired vault protein-like design. (A) Bézier curve aligned to the cross-sectional profile of the vault protein, PDB model 4V60. (B) Spiral-based method applied to the revolution surface of the vault monomer. (C) Staple design, 1% agarose gel after folding, and TEM micrographs with reference-free class averages from single particles (particle sets available in fig. S109). (D) Schematic illustration of the dimer assembly strategy, 1% agarose gel after dimerization, and TEM micrographs with reference-free class averages from single particles (particle sets available in fig. S112). (E) Curvature radius along helices. Color scale from pink (4 nm) to dark blue (30 nm). White bars represent 200 nm.

a design environment for investigating the physical principles, structural properties, and functional behavior of curved and twisted DNA helices—both as they occur in biological systems, with implications for genome organization, gene regulation, and the structural physics of nucleic acids in health and disease, and as components of engineered nanodevices.

References

[1] Rebouças, A. D. S., Silva Filho, J. N. D., Barros, R., Nascimento, Y. R. F. & Coutinho, P. M. Curved bridges live load bending moment distribution using straight and curved girders. *Revista IBRACON de Estruturas e Materiais* **15**, e15208 (2022).

[2] Mateu, M. G. Introduction: The structural basis of virus function. *Structure and Physics of Viruses* **68**, 3–51 (2013).

[3] Aguilar-Planet, T. & Peralta, E. Innovation inspired by nature: Applications of biomimicry in engineering design. *Biomimetics* **9**, 523 (2024).

[4] Loeffler, H. H. *et al.* Reinvent 4: Modern ai-driven generative molecule design. *J Cheminform.* **16**, 20 (2024).

[5] Ong, L. L. *et al.* Programmable self-assembly of three-dimensional nanostructures from 10,000 unique components. *Nature* **552**, 72–77 (2017).

[6] Rothemund, P. W. K. Folding dna to create nanoscale shapes and patterns. *Nature* **440**, 297–302 (2006).

[7] Zeng, Y. C. *et al.* Fine tuning of cpg spatial distribution with dna origami for improved cancer vaccination. *Nature Nanotechnology* (2024).

[8] Oktay, E. *et al.* Dna origami presenting the receptor binding domain of sars-cov-2 elicit robust protective immune response. *Communications Biology* **6**, 308 (2023).

[9] Mills, A. *et al.* A modular spring-loaded actuator for mechanical activation of membrane proteins. *Nature Communications* **13**, 3182 (2022).

[10] Kuzyk, A., Jungmann, R., Acuna, G. P. & Liu, N. DNA origami route for nanophotonics. *ACS photonics* **5**, 1151–1163 (2018).

[11] Franquelim, H. G., Khmelinskaia, A., Sobczak, J.-P., Dietz, H. & Schwille, P. Membrane sculpting by curved dna origami scaffolds. *Nature Communications* **9**, 811 (2018).

[12] Sigl, C. *et al.* Programmable icosahedral shell system for virus trapping. *Nature Materials* **20**, 1281–1289 (2021).

[13] Zhao, Y.-X. *et al.* Dna origami delivery system for cancer therapy with tunable release properties. *ACS Nano* **6**, 8684–8691 (2012).

[14] Dietz, H., Douglas, S. M. & Shih, W. M. Folding DNA into twisted and curved nanoscale shapes. *Science* **325**, 725–730 (2009).

[15] Huang, C.-M., Kucinic, A., Johnson, J. A., Su, H.-J. & Castro, C. E. Integrated computer-aided engineering and design for DNA assemblies. *Nature Materials* (2021). URL `https://doi.org/10.1038/s41563-021-00978-5`.

[16] Veneziano, R. *et al.* Designer nanoscale DNA assemblies programmed from the top down. *Science* **352**, 1534 (2016). URL `http://science.sciencemag.org/content/352/6293/1534.abstract`.

[17] Fu, D. *et al.* Automated design of 3D DNA origami with non-rasterized 2d curvature. *Science Advances* **8**, eade4455 (2022).

[18] Han, D. *et al.* DNA origami with complex curvatures in three-dimensional space. *Science* **332**, 342–346 (2011).

[19] Douglas, S. M. *et al.* Rapid prototyping of 3D DNA-origami shapes with cadnano. *Nucleic acids research* **37**, 5001–5006 (2009).

[20] Kube, M. *et al.* Revealing the structures of megadalton-scale dna complexes with nucleotide resolution. *Nature Communications* **11**, 6229 (2020).

[21] Woo, S. & Rothemund, P. W. Programmable molecular recognition based on the geometry of DNA nanostructures. *Nature chemistry* **3**, 620–627 (2011).

[22] Geary, C. W. & Andersen, E. S. Design principles for single-stranded RNA origami structures. In *International Workshop on DNA-Based Computers*, 1–19 (Springer, 2014).

[23] Castro, C. E. *et al.* A primer to scaffolded DNA origami. *Nature methods* **8**, 221–229 (2011).

[24] Tauvel, P. *Géométrie - 2ème édition* (Dunod, 2005). ENA 9782100494132.

[25] ENSnano. Website. `https://www.ens-lyon.fr/ensnano/`.

[26] ENSnano. Source and binaries. `https://github.com/ensnano/ensnano`.

[27] Annunziato, A. DNA packaging: Nucleosomes and chromatin. *Nature Education* (2008).

[28] Ketterer, P. *et al.* Dna origami scaffold for studying intrinsically disordered proteins of the nuclear pore complex. *Nature Communications* **9**, 902 (2018).

[29] Zhang, Z., Yang, Y., Pincet, F., Llaguno, M. C. & Lin, C. Placing and shaping liposomes with reconfigurable dna nanocages. *Nature Chemistry* **9**, 653–659 (2017).

[30] Mills, A. *et al.* A modular spring-loaded actuator for mechanical activation of membrane proteins. *Nature Communications* **13**, 3182 (2022).

[31] Monferrer, A. *et al.* DNA origami traps for large viruses. *Cell Reports Physical Science* **4**, 101237 (2023).

[32] Thubagere, A. J. *et al.* A cargo-sorting dna robot. *Science* **357**, eaan6558 (2017). URL `https://www.science.org/doi/abs/10.1126/science.aan6558`. `https://www.science.org/doi/pdf/10.1126/science.aan6558`.

[33] Simien, J. M. & Haglund, E. Topological twists in nature. *Trends in Biochemical Sciences* **46**, 461–471 (2021).

[34] Travis, J. The vault guy. *Science* **384**, 1058–1062 (2024).

[35] Van Zon, A., Mossink, M. H., Scheper, R. J., Sonneveld, P. & Wiemer, E. A. C. The vault complex. *Cellular and Molecular Life Sciences (CMLS)* **60**, 1828–1837 (2003).

[36] Berger, W., Steiner, E., Grusch, M., Elbling, L. & Micksche, M. Vaults and the major vault protein: novel roles in signal pathway regulation and immunity. *Cellular and molecular life sciences* **66**, 43–61 (2009).

[37] Buehler, D. C., Toso, D. B., Kickhoefer, V. A., Zhou, Z. H. & Rome, L. H. Vaults engineered for hydrophobic drug delivery. *Small* **7**, 1432–1439 (2011).

[38] Levy, N. & Schabanel, N. Ensnano: a 3D modeling software for DNA nanostructures. In *Proc. of DNA27-27th Int. Conf. on DNA Computing and Molecular Programming* (2021). URL `https://www.ens-lyon.fr/ensnano/`.

[39] Rothemund, P. W. Folding DNA to create nanoscale shapes and patterns. *Nature* **440**, 297–302 (2006).

Materials and Methods

DNA strands Desalted staple strands were purchased from Integrated DNA Technologies (IDT) in water in 96-well plates at a concentration of 100 μM each. The staple strands were pooled and diluted with water to a working concentration of 400 nM each. The different scaffolds used (M13 8064, M13 7560, M13 7249) were purchased from Tilibit Nanosystems. The scaffold (5 nM to 20 nM) and staples ten times in excess were combined in a one-pot reaction with a buffer of 5 mM Tris-HCl, pH=8.0, 1mM EDTA, different concentrations of $MgCl_2$ depending on the origami (12 mM to 20 mM). The thermal annealing ramp was spanned over a time-period from 3.5 hours to 63 hours. The scaffold, concentrations of the components and thermal annealing ramps used for each origami (if not otherwise noted) are described in table T1.

Agarose gel electrophoresis DNA nanostructures visualized by Electron Microscopy were purified from 1% agarose gels (0.5X TBE, 45mM Tris-borate, 1mM EDTA, pH 8.3) supplemented with 11mM $MgCl_2$ and $0.5\text{mg} \cdot \text{ml}^{-1}$ Sybr SAFE. Samples were migrated on the gel for 3h with a running buffer of 0.5X TBE, 11mM $MgCl_2$ $2.85\text{V} \cdot \text{cm}^{-1}$ at room temperature. Bands corresponding to properly folded DNA origami were excised and transferred to a DNA gel extraction spin column (Merck, France) centrifuged at 5,000 g for 5 min at 4°C.

Transmission Electron Microscopy - Negative staining Purified origami were visualized by adsorption onto glow-discharged carbon-coated grid (Quantifoil Micro tools GmbH, Germany), stained for 60 s with a 2% (w/vol) aqueous uranyl acetate (Merck, France) solution, and then dried with ashless filter paper (VWR, France). Observations of EM grids were carried out on a JEM-1400Flash Tungsten microscope working at 120kV, equipped with a GATAN One View camera. Two-dimensional class averages were computed using EMAN2.

Cryo-EM sample preparation The purified and concentrated T6 samples were incubated 5 minutes twice to glow-discharged grids with an ultrathin carbon film supported by a 2/2 carbon film on a 200-mesh copper grid (Quantifoil Micro tools GmbH, Germany). Plunge freezing in liquid ethane was performed with a ThermoFisher Mk-IV Vitrobot with a blot time of 3 s, a blot force of 0 at 15°C and 100% humidity.

Cryo-EM image acquisition Selected grid of T6 was transferred under cryogenic conditions into the TFS Titan Krios TEM with acceleration voltage of 300 kV. Micrographs were acquired in two sessions on the Falcon4i camera under low-dose condition with a total flux of 40 e-/Å2. Data were collected with underfocus values ranging from -0.7 μm to -4.1 μm in nominal resolution of 1.2 Å/px. Automated data acquisition was recorded into 40 individual frames. The forty-frame movies were then globally and locally (5x5 patches, 20% patch overlap) aligned to compensate for drift and beam-induced motion using program motioncor2[40]. The resulting dose-weighted sum of aligned frames was used for subsequent image processing steps, except for estimating the contrast transfer function (CTF) parameters, which were estimated from aligned, non-dose weighted micrographs using the program ctffind4[41,42,43].

Cryo-EM image processing Data processing was done using SCIPION 3.0.9 package[44]. 15,127 dose-weighted micrographs of T6 were used for the processing. The SPHIRE-crYOLO[45] protocol was used for particle picking from a set of 3x binned micrographs. The particles were subjected to three rounds of RELION 2D classification[46,47,48,49] to remove falsely picked grid contaminations and damaged particles, high-quality 2D class averages were selected and duplicated particles with Xmipp3-remove duplicates[50,51] with 80px radius, leaving a set of 142,198 particles. Relion initial model[46,47,48,49] was used for generating the initial 3D volume. First, a 3D refinement without any symmetry (and with the initial model filtered down to 120Å) was applied, producing a 3D map at 26Å and confirming the presence of the expected D6 symmetry. Following this initial refinement, a series of 3D refinements with progressively tightening masks and 3D classifications[46,47,48,49] were applied to get a final set of 72,684 particles, subjected to a final 3D refinement[46,47,48,49] with D6 symmetry, effectively reaching 13Å with a global mask.

Dimerization of the Vault-like origami Each Vault-like monomer was designed to display six anchor staples at its bottom to enable dimerization. Two different versions of the 6 anchor staples A and B were designed with 18-base parts complementary to each other. The sequences of these staples are described in tables T2 and T3. The sequences annealing inside the monomers are in black, the sequences designed to be out of the monomers are in red (two T and the sequence to enable the annealing of staples A

Object	Denaturation phase (15 min) (°C)	Temperature ramp	Hold temperature (°C)	Folding ramp time period (h)	Magnesium chloride concentration (mM)	Scaffold	Scaffold concentration (nM)	Staples concentration (nM)
⌘	65	60°C to 40°C: -1°C/2h	10	42	20	M13 7249	20	200
T1	65	60°C to 40°C: -1°C/2h	10	42	12	M13 7560	20	200
T2	65	1) 60°C to 55°C: -1°C/10min 2) 55°C to 25°C: -1°C/1h	25	33	18	M13 7560	20	200
T3	65	1) 60°C to 55°C: -1°C/10min 2) 55°C to 25°C: -1°C/1h	25	33	18	M13 7560	20	200
T4	65	1) 60°C to 55°C: -1°C/10min 2) 55°C to 25°C: -1°C/1h	25	33	18	M13 7560	20	200
T5	65	60°C to 40°C: -1°C/10min	10	3.5	18	M13 7560	5	50
T6	65	1) 60°C to 55°C: -1°C/10min 2) 55°C to 25°C: -1°C/1h	25	33	18	M13 7560	20	200
DS	65	60°C to 40°C: -1°C/2h	10	42	30	M13 8064	20	200
Vault	65	60°C to 40°C: -1°C/3h	10	63	20	M13 8064	20	200

Table T1: Final folding conditions for each origami.

- Staple no. 1: 5' TTGTTTAACGTCACATT CATTACAAAATGAAAA TT AGTATATAGATAATTAAA 3'
- Staple no. 2: 5' TAACGAGCGTCGATTGCC TT AGTATATAGATAATTAAA 3'
- Staple no. 3: 5' CGACATTCAACCGATCACCGTCAC TT AGTATATAGATAATTAAA 3'
- Staple no. 4: 5' CGGGAACGGATAACCTCCAGTCACGACGTTGT GCCATTC TT AGTATATAGATAATTAAA 3'
- Staple no. 5: 5' CTGGTAATGGGTAAAGGTTTCTTTTTTCGCA TT AGTATATAGATAATTAAA 3'
- Staple no. 6: 5' ATGCCAACGGGAAAGGCTGGCCAGCACCGTCG TT AGTATATAGATAATTAAA 3'

Table T2: Version A of the six staples enabling the dimerization.

- Staple no. 1: 5' TTTAATTATCTATATACT TT TAGCAGCAACTGAACACCCTGA 3'
- Staple no. 2: 5' TTTAATTATCTATATACT TT GTGGTGCGTTACCTGCA 3'
- Staple no. 3: 5' TTTAATTATCTATATACT TT AGGCTGCACTCCAGCCAGCTTTCCGGAACCCGTCGGATTCT 3'
- Staple no. 4: 5' TTTAATTATCTATATACT TT GTTCCGGCAAACGCGGTGTGTACATCGACATAA 3'
- Staple no. 5: 5' TTTAATTATCTATATACT TT CGACTTGACCGTAATCAGTAGCGACAGAATCA 3'
- Staple no. 6: 5' TTTAATTATCTATATACT TT CTCAATCCGCCG GAGCACATCCTCATAACAGCGGATCA 3'

Table T3: Version B of the staples enabling the dimerization.

with staples B, leading to the dimerization of the vault-like origami).

The monomers of the Vault-like origami with staples A and staples B were folded according to the conditions detailed in Table T1. Then, they were purified by agarose gel electrophoresis. Finally, they were assembled in equal concentration for 15 hours at 37°C with 100 mM $MgCl_2$.

References for Material and Methods

[39] Mastronarde, D. SerialEM: A Program for Automated Tilt Series Acquisition on Tecnai Microscopes Using Prediction of Specimen Position. Microscopy and Microanalysis, 9(S02), 1182-1183. doi:10.1017/S1431927603445911 (2003)

[40] Zheng, S. Q. et al. MotionCor2: anisotropic correction of beam-induced motion for improved cryo-electron microscopy. Nat. Methods 14, 331–332 (2017)

[41] Mindell, J. K.; Grigorieff, N. Accurate determination of local defocus and specimen tilt in electron microscopy. J. Struct. Biol. 142/3, 334–347 (2003)

[42] Rohou, A.; Grigorieff, N. CTFFIND4: Fast and accurate defocus estimation from electron micrographs. J. Struct. Biol. 192/2, 216–221 (2015)

[43] Grant, T.; Rohou, A.; Grigorieff, N. (2018) cisTEM, user-friendly software for single-particle image processing. eLife 7:e35383

[44] De la Rosa-Trevín, J. M. et al. Scipion: A software framework toward integration, reproducibility and validation in 3D electron microscopy. J.Struct. Biol. 195, 93–99 (2016)

[45] Wagner, T. et al. SPHIRE-crYOLO is a fast and accurate fully automated particle picker for cryo-EM. Commun Biol 2, 218 (2019)

[46] Zivanov, J. et al., New tools for automated high-resolution cryo-EM structure determination in RELION-3. Elife 7, (2018)

[47] Sjors H.W. Scheres, RELION: Implementation of a Bayesian approach to cryo-EM structure determination, Journal of Structural Biology,

Volume 180, Issue 3, 2012, Pages 519-530, ISSN 1047-8477

[48] Sjors H.W. Scheres, A Bayesian View on Cryo-EM Structure Determination, Journal of Molecular Biology, Volume 415, Issue 2, 2012, Pages 406-418, ISSN 0022-2836

[49] D. Kimanius, B. O. Forsberg, S. HW. Scheres, E. Lindahl, Accelerated cryo-EM structure

[50] De la Rosa-Trevín et al. Xmipp 3.0: An improved software suite for image processing in electron microscopy. J. Struct. Biol. 184 issue 2, 321-328 (2013)

[51] Sorzano, C.O. et al. (2013). Semiautomatic, High-Throughput, High-Resolution Protocol for Three-Dimensional Reconstruction of Single Particles in Electron Microscopy. In: Sousa, A., Kruhlak, M. (eds) Nanoimaging. Methods in Molecular Biology, vol 950. Humana Press, Totowa, NJ. https://doi.org/10.1007/978-1-62703-137-0_11

Acknowledgements:

Fundings: French National Research Agency grant : ANR-22-CE09-0034 (GB); French National Research Agency grant : ANR-22-CE45-0020 (NS); French National Research Agency grant : ANR-19-CE14-0035 (GB); French Centre National de la Recherche Scientifique: INS2I (NS); French Centre National de la Recherche Scientifique: MITI (NS); French Infrastructure for Integrated Structural Biology (GB); French École Normale Supérieure de Lyon (NS); French IXXI Complex System Institute (NS).

Author contributions: Conceptualization: NS, NL, GB, JF, AM; Software: NL, NS, PM, JP, OH, DP; Algorithms: NS, NL; User Interface design: NS, NL, JP; Origami design: NS, NL, GB, JF, AM, GW; Experimental work: JF, AM, AK, GW, AA; Electron microscopy: JF, AM, AK, GW, AA; Data analysis: GB, JF, AM, AK, GW, AA; Visualization: JF, GB; Funding acquisition: GB, NS; Project administration: NS, GB; Writing – original draft: NL, JF, NS, GB; Writing – review & editing: NS, GB, JF, NL, AK, GW.

Competing interests: The authors have no competing interest.

Code and data availability: ENSnano source code is available in the public Github repository[26]; the `.ens` and `.xlsx` files for the designs will be available on an open-source website at the time of publication.

Thanks: The authors thank Olivier Gandrillon at the LBMC lab (ÉNS de Lyon) for granting access to the lab bench, and Catherine Koering and Élodie Vallin for experimental guidance. We thank Josephine Lai Kee Him for help with TEM measurements. We thank the Institut Pasteur in Paris and Eyen for access to TEM facilities and data acquisition.